

## ELASTIC PROPERTIES OF SILICA POLYMORPHS – A REVIEW

#WILLI PABST, EVA GREGOROVÁ

*Department of Glass and Ceramics, Institute of Chemical Technology, Prague (ICT Prague),  
Technická 5, 166 28 Prague 6, Czech Republic*

#E-mail: pabstw@vscht.cz

Submitted May 16, 2013; accepted September 20, 2013

**Keywords:** Silica, Elastic properties, Auxetic materials, Quartz, Tridymite, Cristobalite, Coesite, Stishovite, Silica glass, Young's modulus (Tensile modulus), Shear modulus, Bulk modulus (Compressive modulus), (Negative) Poisson ratio

*The elastic properties of silica phases are reviewed. Available monocrystal data for crystalline SiO<sub>2</sub> polymorphs (low-quartz, high-quartz, low-cristobalite, high-cristobalite, stishovite) are collected from the literature, and effective elastic constants (Young's moduli, shear moduli, bulk moduli and Poisson ratios) are calculated from these using Voigt-Reuss-Hill averaging. Both experimental data and simulation results are taken into account. A table of room temperature elastic constants for crystalline silica polymorphs and silica glass is given that lists the recommended current "state-of-the-art" values. All data are consistent with the well-known auxetic behavior of cristobalite at room temperature, and high-temperature simulation data published for cristobalite confirm auxetic behavior for all temperatures from room temperature up to more than 1500°C. The calculations of this paper show that also quartz can be auxetic, but only in a very limited temperature range around the low-to-high-quartz transition temperature (420 – 577°C). Experimental measurements of elastic properties of tridymite and cristobalite, including high-temperature measurements, are identified as a desideratum of future research.*

## INTRODUCTION

Silica in its diverse polymorphs and subpolymorphs is one of the most remarkable chemical compounds on Earth. Quartz is ubiquitous as a rock-forming mineral, and as a raw material it is indispensable for many branches of industry, e.g. the the glass and ceramic industry, including its refractory branches, and the silicon-based semiconductor industries. Of course, quartz also exhibits remarkable physical properties. In particular, it is well known for much more than a century that quartz exhibits piezoelectric behavior. In fact, the piezoelectric effect was discovered on quartz by Pierre Curie (1859 - 1906) and Paul-Jacques Curie (1855 - 1941) in 1880 (and the converse effect in 1881), and in 1910 Paul-Jacques Curie performed the first determination of the piezoelectric constant of quartz [1]. Subsequently, following the first treatment of the phenomenological theory of piezoelectricity based on thermodynamic principles proposed by Lord Kelvin (William Thomson, 1824 - 1907), the phenomenological theory of piezoelectricity was elaborated more completely by Pierre Duhem (1861-1916) and others [1], but most fully and rigorously in 1894 by Woldemar Voigt (1850 - 1919), who with his "Lehrbuch der Kristallphysik" (1910 and 1928) laid the foundations of crystal physics in general and pioneered the use of tensor formalism for the description of the physical properties of anisotropic materials, in particular monocrystals.

Due to the interest in quartz as a piezoelectric material during the 20<sup>th</sup> century, the elastic properties of quartz at and around room temperature are very well known. Precise values are available for monocrystals of low-temperature quartz, from which those of polycrystalline aggregates can be readily calculated. However, for elevated temperatures (a few hundred °C) experimental data are much less frequent, and the situation is even worse for other polymorphs of silica (except for silica glass). Nevertheless, due to the interest in geophysics, e.g. seismology and using silica phases as natural "thermometers" or "barometers" in geological contexts, some high-temperature and high-pressure polymorphs of silica have been investigated quite thoroughly. Unfortunately, the silica phase that are of primary interest in ceramic science and technology, viz. tridymite and cristobalite, are the least studied so far, although cristobalite is a quite common crystalline silica phase in ceramic microstructures and, together with tridymite, forms the basis of a whole group of refractory products, so-called silica refractories. Fortunately, during the last two decades, the interest in cristobalite has grown because of the discovery of its auxetic behavior. However, still much work remains to be done for the high-temperature properties of cristobalite, and the elastic properties of tridymite at high temperatures have remained tabula rasa until now, although they are critical e.g. for the application of silica bricks.

It has to be emphasized that, apart from the evident fact that elastic properties are key mechanical properties of their own, they determine the maximum strength and hardness of materials and significantly affect the thermal shock behavior of materials. Moreover, only a knowledge of the components of the elasticity tensor (elements of the stiffness matrix) of the corresponding monocrystals allows a reliable calculation of the theoretical elastic constants of dense polycrystalline aggregates, which is again the basic input information for efficient property prediction in dependence of the microstructure, e.g. porosity. Therefore, it is the aim of this study to collect current knowledge on the elastic properties of silica phases, i.e. mainly the knowledge that has accumulated during the 20<sup>th</sup> century, and thus implicitly to show the flaws that still exist and to indicate the desiderata of future research.

## THEORETICAL

### A shortcut through silica phases

Silica (SiO<sub>2</sub>) occurs in many polymorphic modifications (polymorphs and subpolymorphs) and polytypes, and in the amorphous (glassy) state. Petzold [2] has listed 12 silica phases (11 crystalline ones and silica glass), Salmang and Scholze [3] 14 (including melanophlogite and a hexagonal high-pressure phase at pressures > 35 GPa) and some authors, following Sosman's "gedankenexperiment" [4,5], even more than 20 [6,7]). Except for several amorphous phases (apart from the "normal" silica glass e.g. "compact vitreous silica", "super-piezo-vitreous silica" and so-called

"silica M", amorphized by fast neutrons [5,7]), the main point of dispute has been the number of tridymite phases (or "forms"), which ranges – depending on the author – from two [8-10] to three (most authors), five [11] and nine [5,7].

Table 1 gives an overview of the most important silica phases, together with their symmetry and density. In accordance with the majority of authors we have chosen to subdivide tridymite here into three sub-polymorphs, but the medium-temperature "middle"-tridymites may contain several more or less similar forms (sometimes classified as low- or high-temperature polymorphs) with transition temperatures ranging from 64°C to 475°C [5] or at least from 100 to 400°C [3]. However, the behavior of tridymite samples is variable and in some cases transitions have been observed in the temperature range 80 - 270°C [12]. According to some authors [13], the hexagonal high-tridymite occurs only at temperatures above 420°C. In fact, despite occasional experimental evidence of the contrary [14,15], it is commonly acknowledged today, that tridymite does not exist as a pure silica phase [2, 16-21] and that sodium ions are the most effective stabilizers for the tridymite lattice, because they are smaller than potassium but do not reduce the eutectic temperature below 870°C, as e.g. lithium [3, 22-24]. Nevertheless, with respect to the fact that the impurity content necessary for tridymite formation is very low, it is common practice to list tridymite together with the other silica phases, and we follow this tradition. Tridymites with high contents of foreign ions are considered as "stuffed derivatives" of silica [2, 21].

From the viewpoint of glass and ceramic technology (including refractories) the most important of these are

Table 1. Symmetry and density of the most important crystalline silica polymorphs and silica glass according to the textbook literature [2, 3, 5, 7, 10, 11, 21, 25-27].

Silica phase	Crystal system	Point group (crystal class)	Space group	Density (g/cm <sup>3</sup> )
Low-quartz	trigonal	32	P 3 <sub>2</sub> 21 or P 3 <sub>1</sub> 21 (enantiomorphic)	2.65
High-quartz (> 573°C)	hexagonal	622	P 6 <sub>2</sub> 22 or P 6 <sub>4</sub> 22 (enantiomorphic)	2.53
Low-tridymite	monoclinic	m	C c	2.26-2.27
Middle-tridymites (> 100 - 120°C, > 160 - 180°C)	orthorhombic (pseudo-hex., possibly several phases with transition temperatures 64, 117, 163, 210 and 475°C)	222	C 222 <sub>1</sub>	2.24-2.29 [3, 5, 10, 11, 26-27]
High-tridymite (> 200 - 450°C)	hexagonal	6/m 2/m 2/m	P 6 <sub>3</sub> /m m c	2.22-2.26
Low-cristobalite (< 200 - 270°C)	tetragonal	422	P 4 <sub>1</sub> 2 <sub>1</sub> 2	2.32
High-cristobalite (> 200 - 270°C)	cubic	4/m $\bar{3}$ 2/m	F d $\bar{3}$ m	2.20
Silica glass	amorphous	–	–	2.20
Coelite (> 300 - 800°C and 1.5 - 4 GPa)	monoclinic	2/m	C 2/c	≈ 3.0
Stishovite (> 1000 - 1200°C and 10 - 13 GPa)	tetragonal	4/m 2/m 2/m	P 4 <sub>2</sub> /m n m	≈ 4.3

quartz, tridymite, cristobalite and silica glass. Their main importance consists in the fact that they are important raw materials (quartz in the form of sand, sandstone, quartzite and rock quartz), the major phases in silica refractories (tridymite and cristobalite) and a very important special product (silica glass), irreplaceable for laboratory ware and many applications requiring low thermal expansion and high thermal shock resistance. Apart from that, cristobalite (but not tridymite) is a quite common phase occurring in traditional silicate ceramic microstructures after firing.

While quartz is ubiquitous in nature (it forms about 15 % of the Earth's crust [28]), tridymite and cristobalite are rarely found in nature (however, originally they have been found in natural deposits by von Rath in 1861 - 1868 and 1884 - 1887, respectively – cristobalite draws its name from San Cristobal in Mexico [9, 29]) and the same holds true for silica glass, which may occasionally occur (as so-called “lechatelierite”, named after Henri Le Chatelier) in tectites and fulgurites. The high-pressure polymorphs coesite (discovered by Coes [30]) and stishovite (discovered by Stishov and Popova [31]) are of importance in geophysics and have greatly influenced our understanding of the Earth mantle [21]. They also occur in meteorite impacts craters [8] and can be artificially made by high pressure synthesis, but are not used in technical applications.

Beside the phases listed in Table 1 there are other crystalline silica phases of minor importance, such as keatite (also called “silica K”, a tetragonal form of  $\text{SiO}_2$  with density  $2.50 \text{ g/cm}^3$ , stable under hydrothermal conditions, discovered by Keat [32]), melanophlogite (a tetragonal form of  $\text{SiO}_2$  with density  $2.05 \text{ g/cm}^3$ , possibly containing organic traces, discovered by Lasaulx in 1876 [29]) and crystalline fibrous silica (also called “silica W”, an orthorhombic form of  $\text{SiO}_2$  with density  $1.97\text{--}1.98 \text{ g/cm}^3$ , formed by disproportionation from the gas phase [33]), see also [2, 3, 5, 7, 8, 21, 26]. More recently, also a “post-stishovite” silica phase (with a density even higher than stishovite) has been predicted by computer simulation (molecular dynamics) [34] and another high-pressure silica phase with  $\text{CaCl}_2$  structure (at pressures beyond those necessary for stishovite) has been proposed as well and is expected to transform to another silica with orthorhombic  $\alpha\text{-PbO}_2$  structure at pressures higher than approx. 115 GPa [35]. Of course all these very-high-pressure silica polymorphs are of significance only in geophysics (and cosmophysics).

Chacedony and chert are very fine grained (micro- or nanocrystalline, sometimes called “cryptocrystalline”) compacts of polycrystalline quartz. Moganite is a more recently discovered microcrystalline form of silica [21, 36]. In contrast to these “anhydrous” silica types, pristine opal is a “hydrated” form of silica containing variable amounts of molecular water and consists of regions with regular packing arrangement of submicron silica (quartz) spheres with a diameter of 150 - 300 nm [10]. Opals may

contain also tridymite and cristobalite in minor amounts, indicating their formation in hydrothermal low-pressure environments under elevated temperatures.

#### Structure and phase transitions of high-temperature silica polymorphs

It is well known that the high-temperature (low-pressure) silica polymorphs tridymite and cristobalite are formed upon heating by slow and sluggish phase transformations (so-called “reconstructive” transformations [37] or “heterogeneous polymorphic phase transitions of first order” [38]), when quartz is heated to sufficiently high temperatures. The equilibrium transition temperature reported for the formation of tridymite by heating of quartz is  $867\text{--}870^\circ\text{C}$  [3, 7, 39], but this temperature holds only in the presence of foreign ions (see above). In this case the transition from tridymite to cristobalite occurs at a temperature of  $1470^\circ\text{C}$ . If foreign ions are not present, tridymite does not occur and quartz transforms above  $1000\text{--}1050^\circ\text{C}$  slowly, via a transient phase of unknown (XRD amorphous) structure [40], to cristobalite [2, 3, 17, 25]. Even in the presence of foreign ions, however, it is not tridymite but cristobalite that is formed in the first place when quartz is heated to temperatures higher than  $870^\circ\text{C}$  (usually higher than  $1000\text{--}1200^\circ\text{C}$ , i.e. in the middle of the stability range of tridymite, which is  $870\text{--}1470^\circ\text{C}$ ), since according to “Ostwald's step rule” [2] the higher-energy (metastable) polymorph cristobalite is formed first and the low-energy (stable) polymorph tridymite is formed from the latter only after a relatively long time [3, 21, 41-44]. In the refractory industry silica bricks are typically made from crushed and milled quartzite mixed with lime wash (as a CaO source) by firing at  $1400\text{--}1500^\circ\text{C}$  for 160 – 330 hours [27]. When the firing temperature is approximately  $1450^\circ\text{C}$ , the resulting tridymite-to-cristobalite ratio is around unity (45 - 50 wt. % each), but it can be shifted to a higher value (more tridymite) when the content of impurities is higher [45]. During long-term operation of the high-temperature aggregate, the tridymite-to-cristobalite ratio can increase (this kinetically inhibited and thus slow process is called “tridymitization”).

Once formed, the high-temperature polymorphs tridymite and cristobalite do not transform back to quartz in time-scales of engineering interest, but they undergo rapid “displacive” phase transformations (also classified as “lambda ( $\lambda$ ) transitions”, see e.g. [3], or as “homogeneous polymorphic phase transitions of second or higher order” [38], see [21]) to their low-temperature subpolymorphs. These displacive transformations between high- and low-temperature subpolymorphs (within one and the same main polymorph, i.e. tridymite or cristobalite) are completely reversible, similar as in the case of quartz, where this displacive transformation takes place at  $573^\circ\text{C}$ . The displacive transformations can be sharp and unique (as in the case of the transition

from low- to high-quartz), or consist of a sequence of two or more transitions (as in the case of tridymite), or exhibit a “hysteresis” (difference in the transition temperatures) between heating and cooling (as in the case of cristobalite, where this hysteresis can be up to 30 K [3, 46]). This hysteresis has been explained by different nucleation barriers during heating (i.e. in low-cristobalite) and cooling (i.e. in high-cristobalite) [3]. It is believed to depend on stresses originating from structural disorder [47] and is small when the degree of disorder is high [3]. Freshly formed cristobalite is known to behave differently during heating and cooling [3]: during the first cooling the linear contraction is only 0.5 % (because microcracks counterbalance part of the contraction), while during the subsequent heating the linear expansion can be as high as 1.4 % [48]. The average volumetric contraction (or expansion) during the transition from low- to high-cristobalite is 2.8 % [3].

Although the phase transitions can be investigated by various methods, e.g. impulse excitation or resonant frequency techniques for recording the temperature dependence of elastic properties, differential thermal analysis (DTA) and dilatometric measurements have traditionally been the most popular methods used to study the phase transitions between low- and high-temperature subpolymorphs. The DTA effects of low-to-high-temperature subpolymorphs of quartz, cristobalite and tridymite are all reported to be reversible, sharp and endothermic during heating (i.e. exothermic during cooling) [49]. The transition temperature for quartz is 573°C (although certain indications of the phase transitions – diffuse X-ray diffraction peaks – are visible during heating already from 400°C [2, 25, 50] and the onset temperature of the DTA peak is reported to be 550°C [49]), while for cristobalite usually a temperature range is reported that differs to a certain degree: usually 200 - 270°C, but sometimes also 200 - 280°C [9], 220 - 260°C [49], 230 - 270°C [26] or a temperature around 230°C [2, 25], and some authors attribute the temperature difference to the hysteresis between heating (275°C) and cooling (241°C) [11].

The structure of cubic high-cristobalite can be viewed as a three-layer structure with a layer sequence analogous to the face-centered cubic densest packing, i.e. ABCABC..., while the hexagonal high-tridymite can be viewed as a two-layer structure with the layer sequence ABAB... [3, 13, 21, 51, 52]. However, tridymite is an intricate and problematic phase. Broadened and diffuse XRD peaks are frequently observed [3] and have been interpreted as stacking faults [52] and the different stacking sequences as polytypism [20]. That means, tridymite always contains a certain amount of three-layer sequences and thus there is a gradual transition between the structures of (high-) “tridymite” sensu lato (prevailing two-layer type) and (high-)”cristobalite” sensu lato (prevailing three-layer type) [18] and the distinction between the two phases sensu stricto may

become unjustified [3, 21, 53]. More recently, also neutron diffraction has confirmed this view and contributed to a more sophisticated view on the differences between low- and high-cristobalite [54, 55]. Similar, magic angle spinning nuclear magnetic resonance (MAS-NMR) using <sup>29</sup>Si has been applied to investigate the tridymite superstructures [56], resulting in transition temperatures of 108°C (monoclinic to first orthorhombic), 165°C (first to second orthorhombic) and 206°C (second to third orthorhombic). According to these studies, the third orthorhombic phase is high-tridymite and, interestingly, it is the second, not the third orthorhombic phase that is pseudohexagonal and thus closest to the hexagonal high-temperature phase [21].

The structure of low-cristobalite is known to be tetragonal with lattice constants close to the cubic form [3], while low-tridymite is usually considered as monoclinic (although some authors have also reported on a triclinic phase [57]) and the “medium-tridymite” as orthorhombic (either pseudohexagonal with lattice constants close to the hexagonal form [58] or two other orthorhombic forms [59]). Important structural characteristics of the silica phases are the Si–O distance (mostly ≈ 161 pm, slightly lower – 155 pm – only for low- and medium-tridymite, significantly higher – up to 187 pm – only for stishovite and fibrous silica), the Si–O–Si bond angle (mostly ≈ 144–145° for silica phases and silicates, but ranging from approximately 140 to 180°) [3, 9, 21].

The melting temperature of cristobalite is 1720 ± 10°C [3, 11, 21, 26, 28], but quartz begins to melt (very slowly from the surface) at temperatures as low as 1400 - 1450°C [26, 60, 61]. However, the rate is extremely low, and even at 1750°C the melting rate of quartz is only 100 nm/s [3]. That means, quartz can easily be superheated. The melting temperature of tridymite is approximately 1670 ± 10°C [2, 26].

Theoretical considerations on elastic  
property calculations and measurements,  
with special regard to silica phases

The elastic properties of anisotropic materials in deformation processes for which Hooke’s law can be assumed to be valid are characterized by the stiffness tensor, which is a fourth-order tensor. In the most general case the maximum number of independent elastic constants is 21 for triclinic monocrystals. For materials of higher symmetry the number of independent elastic constants is decreased, from 13 for monoclinic monocrystals to 9 for orthorhombic, 6 for trigonal and tetragonal, 5 for hexagonal and 3 for cubic monocrystals [62]. For isotropic materials the number of independent elastic constants is two. That means, when two independent elastic constants are known for isotropic monocrystals, any other elastic constant, e.g.

one that is convenient for the problem in question, can be calculated. For example, the Young modulus  $E$  can be calculated from the bulk modulus  $K$  and the shear modulus  $G$  via the relation

$$E = \frac{9KG}{3K + G} \quad (1)$$

and the Poisson ratio  $\nu$  can be calculated from the bulk modulus and the shear modulus via the relation

$$\nu = \frac{3K - 2G}{6K + 2G} \quad (2)$$

The latter relation is interesting, because it indicates the conditions, under which a material can be auxetic, i.e. have a negative Poisson ratio. For incompressible materials the bulk modulus (compressive modulus) approaches infinity ( $K \rightarrow \infty$ ) and thus the Poisson ratio approaches a value of 0.5. On the other hand, when the bulk modulus approaches zero ( $K \rightarrow 0$ ), i.e. the material is “infinitely compressible”, the Poisson ratio tends toward  $-1.0$  [63].

The calculation of effective elastic constants of dense polycrystalline aggregates with isotropic microstructure (i.e. random orientation of crystallites) from the elastic constants of monocrystals (i.e. the elements of the stiffness matrix) has been described elsewhere in great detail [64, 65] and will not be repeated here. In essence, the procedure consists in an orientational averaging of the single crystallites via the Voigt and Reuss bounds (i.e. invoking isostrain and isotress assumptions) [66, 67] and subsequent simple arithmetic averaging of the two values [68] to obtain the so-called Voigt-Reuss-Hill average [69]. This is considered as the final value.

Of course, the procedure sketched above is valid for isothermal and adiabatic elastic constants, but the two data sets should in principle not be intermingled. From time to time authors seem to have doubts about the magnitude of the difference between isothermal elastic constants (obtained from static or quasistatic measurements)

and adiabatic elastic constants (obtained from dynamic measurements). In many cases the difference is overestimated or even deliberately overemphasized to tentatively explain otherwise unexplainable differences in experimental data. Therefore, and with special regard to the purpose of this paper, we would like to comment on this point here. Of course, thermodynamic considerations are necessary for the material considered.

The difference between isothermal and adiabatic (= isentropic) elastic constants, measured via static and dynamic techniques, respectively, can be calculated for any temperature in question as soon as the ratio of specific heats at constant pressure and constant volume is known for that temperature [70, 71]. For this purpose, the difference between the specific heat at constant pressure  $c_p$  and the specific heat at constant volume  $c_v$  can be calculated according to the thermodynamic relation [71-73]:

$$c_p - c_v = TVK(3\alpha)^2, \quad (3)$$

where  $V$  the specific volume,  $T$  the absolute thermodynamic (Kelvin) temperature,  $K$  the isothermal bulk modulus and  $\alpha$  the (true) coefficient of (linear) thermal expansion (all quantities for the temperature in question). Note that here we have replaced the volumetric (cubic) coefficient of thermal expansion by three times the linear one. Of course, strictly speaking this is an approximation ( $\alpha_{\text{volumetric}} \approx 3\alpha$ ), but with respect to the small absolute values of the thermal expansion coefficients (order of magnitude  $10^{-5} \text{ K}^{-1}$ ), this approximation is absolutely adequate. Dividing both sides by  $c_v$ , replacing  $V$  by the inverse density  $1/\rho$  and the isothermal bulk modulus using the relation [70]

$$\frac{\tilde{K}}{K} = \frac{c_p}{c_v} \quad (4)$$

we obtain for the ratio  $c_p/c_v$

$$\frac{c_p}{c_v} = 1 + \frac{TK(3\alpha)^2}{\rho c_v} = 1 + \frac{T\tilde{K}(3\alpha)^2}{\rho c_p} \quad (5)$$

Invoking the fact that the isothermal shear modulus equals the adiabatic one, all elastic constants of isotropic materials, including the Young's modulus and the Poisson ratio can be calculated in their isothermal and adiabatic variants.

Figure 1 shows the temperature dependence of the specific heat for the different silica phases [3]. It is evident that – except for the phase transitions of quartz and tridymite – the specific heat exhibits a monotonic increase and that it approaches for high temperatures the value calculated according to the Dulong-Petit rule [72] or – more precisely – the Neumann-Kopp rule [73], which is for  $c_p$  approximately

$$c_p = 26.8 \cdot \frac{n}{M} \quad (6)$$

(in  $\text{J}/(\text{gK})$ ; for  $c_v$  the numerical constant would be 25.1 [72]), where  $n$  is the number of elements in a formula

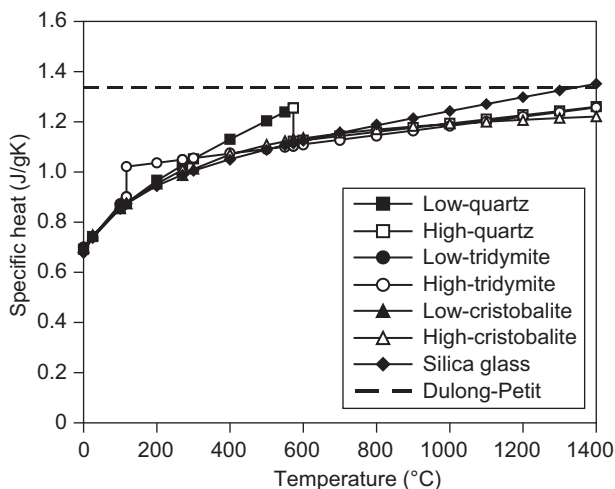


Figure 1. Temperature dependence of the specific heat of silica phases, based on data from [3].

unit (= 3 for SiO<sub>2</sub>) and M is the molar mass (= 60.1 g/mol for SiO<sub>2</sub>). According to this rule the asymptotic value for SiO<sub>2</sub> is 1.34 J/(gK).

Table 2 lists the relevant data for calculating the ratio  $c_p/c_v$  for silica phases at different temperatures [3]. The adiabatic bulk moduli are taken from the room temperature values recommended at the end of this paper (see below) and the high-temperature data available in the literature for low-quartz and silica glass [74, 75]. The thermal expansion coefficients are from [3]. The uncertainty of these values is generally the dominant source of error in this calculation.

Note that the specific heat ratio  $c_p/c_v$  is at the same time the ratio between the adiabatic and isothermal bulk modulus (see above). It is evident that the adiabatic bulk moduli differ from the isothermal values usually by 0.3 - 1.4 % (for silica glass the difference is even much lower, viz. < 0.005 %), only in the vicinity of phase transition the difference can be significantly larger (e.g. 13.8 % for low-quartz at 550°C), due to the extremely high coefficient of thermal expansion in this region. It follows from the theory of thermoelasticity that there is no difference between adiabatic and isothermal shear moduli [70]. Therefore, when the shear moduli are known, the differences between adiabatic and isothermal Young's moduli and Poisson ratios can be calculated as well. The results are listed in Table 3.

The adiabatic Young's moduli differ from the isothermal ones usually by less than 0.5 %, only in the close vicinity of the phase transition the difference is higher

(e.g. 5.9 % for low-quartz at 550°C). In the case of the Poisson ratio the differences between adiabatic and isothermal values are usually higher (except for the case of silica glass where the difference is extremely small, < 0.007 %!) and can easily achieve values of 3 - 5 %. Of course, in the vicinity of phase transitions the difference can be much higher (e.g. 24.5 % for low-quartz at 550°C). Moreover, in contrast to the other elastic constants (moduli), where the adiabatic values are always higher (or equal in the case of the shear modulus), the adiabatic Poisson ratios can be lower or higher than the isothermal ones. It has to be emphasized that the crystalline high-temperature polymorphs of silica, i.e. high-quartz, high-tridymite and high-cristobalite have zero or even slightly negative coefficients of thermal expansion (and very small absolute values) [3]. Therefore the difference between adiabatic and isothermal elastic constants will be absolutely negligible for these phases (even smaller than for silica glass), and the values in Table 3 can be considered as "worst case estimates".

#### Elastic properties of silica glass

Silica glass has a density of approx. 2.20 g/cm<sup>3</sup> (values from approx. 2.02 to 2.21 are reported in the literature, but the lower values refer mostly to opaque silica glass containing bubbles [7, 76]). The thermal expansion coefficient is known to be very low for silica glass, and a value of approx.  $0.5 \times 10^{-6} \text{ K}^{-1}$  seems to be

Table 2. Relevant data for the calculation of the ratio  $c_p/c_v$  at different temperatures; the isothermal bulk modulus has been calculated (room temperature bulk moduli from the table of recommended values at the end of this paper, high-temperature data from [74, 75], thermal expansion coefficients from [3]).

Silica phase	Temp. (°C)	Specific heat $c_p$ (J/gK)	Density $\rho$ (g/cm <sup>3</sup> )	Coefficient of thermal expansion ( $10^{-6} \text{ K}^{-1}$ )	Adiabatic bulk modulus (GPa)	Specific heat ratio $c_p/c_v$	Isothermal bulk modulus (GPa)
Low-quartz	25	0.742	2.65	12.3	38.3	1.008	38.0
Low-tridymite	25	0.742	2.26	21.0	19.7	1.014	19.4
Low-cristobalite	25	0.748	2.32	10.3	16.3	1.003	16.3
Silica glass	25	0.737	2.20	0.5	36.3	1.00002	36.3
Low-quartz	550	1.239	2.59	56.7	18.6	1.138	16.3
Silica glass	550	1.107	2.1985	0.5	42.2	1.00003	42.2
Silica glass	1000	1.243	2.197	0.5	43.2	1.00005	43.2

Table 3. Adiabatic and isothermal Young's moduli and Poisson ratios, calculated using the shear moduli (room temperature values from the table of recommended values at the end of this paper, high-temperature data from [74, 75]).

Silica phase	Temp. (°C)	Shear modulus (GPa)	$\tilde{E}$ (GPa)	$E$ (GPa)	Ratio $\tilde{E}/E$	$\tilde{\nu}$	$\nu$	Ratio $\tilde{\nu}/\nu$
Low-quartz	25	41.1	95.6	95.4	1.0022	+ 0.084	+ 0.082	1.029
Low-tridymite	25	28.8	58.1	57.8	1.0046	+ 0.009	+ 0.004	2.154
Low-cristobalite	25	39.1	65.2	65.1	1.0012	- 0.166	- 0.167	0.994
Silica glass	25	30.9	72.2	72.2	1.00003	+ 0.168	+ 0.168	1.000
Low-quartz	550	42.4	72.2	68.2	1.0597	- 0.148	- 0.196	0.755
Silica glass	550	33.4	79.3	79.3	1.00007	+ 0.187	+ 0.187	1.000
Silica glass	1000	35.9	84.4	84.4	1.00001	+ 0.175	+ 0.175	1.000

a useful approximation for most practical purposes, at least up to temperatures around 1000°C [7, 76]. Using this value, the decrease of density with increasing temperature can be quite reliably predicted using the approximation that the volumetric thermal expansion coefficient is three times the linear one, see Figure 2. Recently, the elastic properties of silica glass have been investigated experimentally by Brillouin scattering, in

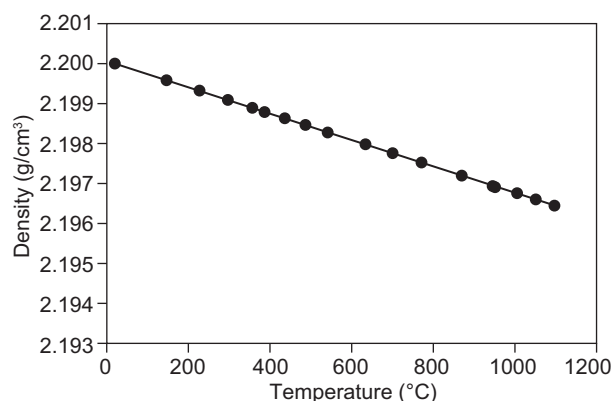


Figure 2. Temperature dependence of the density of silica glass, based on data in [74].

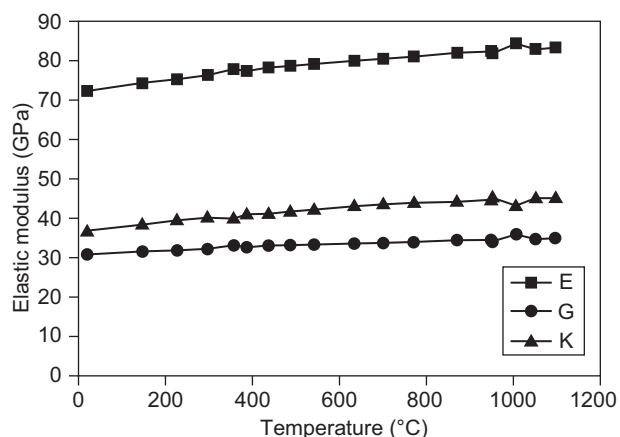


Figure 3. Temperature dependence of the elastic constants of silica glass, calculated from the sound velocities listed in [74].

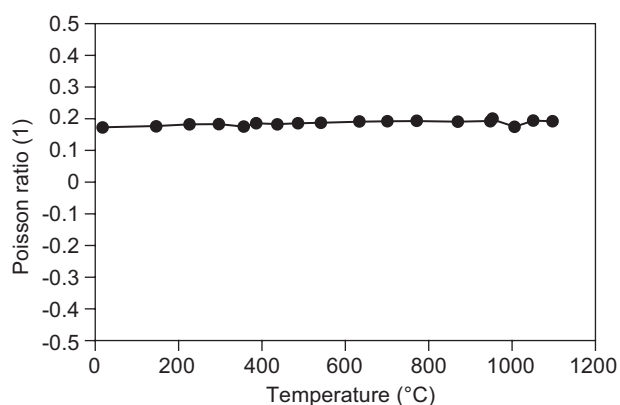


Figure 4. Temperature dependence of the Poisson ratio of silica glass, calculated from the sound velocities listed in [74].

which sound velocities are calculated from changes in the refractive index. Figure 3 shows the temperature dependence of the elastic moduli  $E$ ,  $G$  and  $K$ , calculated from the sound velocities listed in [74]. It is evident that between room temperature and 1000°C all three elastic moduli exhibit a monotonic increase ( $E$  from 72.3 to 84.4 GPa,  $G$  from 30.8 to 35.9 GPa and  $K$  from 36.9 to 45.2 GPa). This increase of the elastic moduli of silica glass with temperature, which is contrary to most other glasses [7], has been confirmed by a number of authors [77-80]. The room temperature values are in excellent agreement with the range of values cited in the literature (for  $E$  70.6 - 73.5 GPa [7, 81, 82] and 68.6 - 73.5 GPa [76], for  $G$  30.2 - 31.5 GPa [7, 82]). According to the sound velocities listed in [74] the Poisson ratio  $\nu$  increases from 0.173 at room temperature to 0.198. Thus, it exhibits a slightly increasing trend with increasing temperature, and the room temperature value is again in excellent agreement with the commonly accepted range of 0.158 - 0.17 [7, 76, 81-83]. Clearly, all elastic constants depend on the density. In particular, it has been reported in the literature that the shear modulus  $G$  decreases by 0.7 % (from 31.37 to 31.15 GPa) and the Poisson ratio  $\nu$  increases by 5.5 % (from 0.162 to 0.173) when the density increases by 0.1 % (from 2.201 to 2.203 g/cm<sup>3</sup>) [6].

#### Elastic properties of crystalline silica polymorphs

##### Quartz

Quartz occurs in two modifications (low- and high-temperature subpolymorphs), a trigonal low-temperature modification (point group 32) and a hexagonal high-temperature modification (point group 622). Although the notation by Greek characters is not unique in the literature (e.g. in the geological-mineralogical literature  $\alpha$  is usually preferred to denote the low-temperature modification), we recommend – if Greek characters are to be used at all – to use  $\alpha$  for the high-temperature modification and  $\beta$  for the low-temperature modifications, because then the reconstructive phase transitions between the main polymorphs (quartz, tridymite and cristobalite) can be considered as being exclusively between  $\alpha$ -subpolymorphs, even if (as in the case of tridymite) there are more than 2 subpolymorphs. An alternative that avoids this confusion altogether is to using the handy terms “low-quartz” and “high-quartz” (and similarly “low-cristobalite” and “high-cristobalite”; with regard to the somewhat disputable status of tridymite phases it makes sense to distinguish also a “high-tridymite” and denote the remaining phases, irrespective of how many they may be, as “low-tridymite”). Due to the screw-like structure along (or around) the  $c$ -axis, which is responsible for optical activity, both low-quartz ( $\beta$ -quartz) and high-quartz ( $\alpha$ -quartz) exist in two enantiomorphic forms (left- and right-handed, space groups  $P3_221$  or

P3<sub>1</sub>21 and P6<sub>2</sub>22 or P6<sub>4</sub>22). Since only the point group (crystal class), not the space group, is responsible for the symmetry of (thermo-)mechanical properties, both enantiomorphic forms are equivalent from the viewpoint of (thermo-)mechanical properties. In fact, when only elastic properties are considered, these are completely determined by the crystal system and – in contrast to widespread belief – more detailed information, e.g. the knowledge of the crystal class, is not required. We recall that more than a decade ago, it has been proved that trigonal and tetragonal classes with 7 independent elastic constants do not exist [84], see also [62]. Thus, low-quartz (trigonal) has 6, while high-quartz (hexagonal) has 5 independent elastic constants. Table 4 lists the independent components of the stiffness tensor (elasticity tensor) as determined by different authors. Mean values are calculated here to extract final recommendable values for the individual stiffness components based on experimental measurements and standard deviations should be considered as a rough guide to assess the reliability (not the precision) of these mean values calculated from published literature data. Both values will be used for comparing published experimental data with the published computer simulation results below.

From the early measurements of elastic constants, the calculated Poisson ratios of quartz are in the range 0.119 - 0.135 [1, 95, 96]. More data on the elastic properties of quartz and other forms of silica can be found in the books of Sosman [97] and Joffé [98].

More recently, computer calculations of the elastic constants of quartz and other silica phases have been performed using molecular dynamics (MD) simulations, i.e. molecular-level atomistic modeling using interatomic potentials [99, 100], or density functional theory (DFT) [101, 102] and other methods such as lattice dynamics (LD) [103, 104]. The interest in these calculations is in the case of silica phases partially triggered by the fact that isotropic aggregates of cristobalite – and in a

certain temperature range also quartz – exhibit auxetic behavior, i.e. negative Poisson ratios [63, 93, 104-112]. The first MD simulations of silica polymorphs used empirical force fields based on the rigid ion model (unsuccessful) and the shell model (successful) [103]. A first breakthrough in the field of nonempirical molecular modeling (based on ab initio calculation for small clusters) was the proposition of a relatively successful [113] two-body potential for silica by Tsuneyuki, Tsukada, Aoki and Matsui (so-called “TTAM potential”) [114], which has later been applied e.g. for lattice dynamic calculations of vibrational frequencies in low-quartz, low-cristobalite, coesite and stishovite [115]. Another, even more successful, two-body potential containing three terms (exponential repulsion, dispersive attraction and long-range electrostatic interactions) has been proposed by van Beest, Kramer and van Santen (so-called “BKS potential”) [116] and used for calculating the structure and the elastic constants of low-quartz, high-quartz, low-cristobalite and the high-pressure silica polymorph stishovite [117, 118]. Ab initio (first principles) calculations based on density functional theory (DFT), using the projector-augmented-wave method (PAW) or the plane-wave pseudo-potential method (PWPP) method, both within the local-density approximation (LDA), have also been applied to calculate the structure (lattice constants, unit cell volume, density, and radial distribution functions of Si–O and O–O distances as well as Si–O–Si and O–Si–O bond angles) and elastic constants of low-quartz and low-cristobalite [112, 119]. Similar DFT calculations under LDA approximation have been performed with two variants of Troullier-Martins type pseudopotentials (termed KA and FHI, respectively) and used to predict the elastic constants of low-quartz, low-cristobalite, high-cristobalite, stishovite and other important ceramic phases such as  $\alpha$ -Al<sub>2</sub>O<sub>3</sub> and  $\beta$ -Si<sub>3</sub>N<sub>4</sub> [120]. Table 5 lists the elastic constants calculated on the basis of these

Table 4. Independent components of the stiffness tensor (GPa) for low-quartz from experimental measurements at or around room temperature (0 - 35°C); isagric values are corrected for piezoelectric effects, see [1].

No.	Type of constant (experimental method)	$C_{11}$	$C_{12}$	$C_{13}$	$ C_{14} $	$C_{33}$	$C_{44}$	Reference
1	Isothermal (static)	85.1	6.96	14.1	16.9	105.4	57.1	[85]
2	Adiabatic (calculated from 1)	85.4	7.26	14.4	16.9	105.6	57.1	[1], based on [85]
3	Adiabatic isagric (resonant frequency)	86.75	6.87	11.3	17.96	106.8	57.86	[86, 87]
4	Adiabatic (resonant frequency)	86.05	5.05	10.45	18.25	107.1	58.65	[88]
5	Adiabatic (calculated from isothermal)	87.5	7.62	15.1	17.2	107.7	57.3	[1], based on [89]
6	n.a.	87.26	7.65	14.68	17.03	107.63	57.04	[90]
7	Adiabatic (ultrasonic wave velocities)	86.8	7.0	19.1	18.0	105.8	58.2	[91]
8	n.a.	86.74	6.98	11.9	17.9	107.2	57.9	[92]
9	Adiabatic (resonant frequency)	87.7	6.8	12.3	18.7	106.3	59.0	[93]
10	Adiabatic (Brillouin scattering)	87	7	13	18	107	57	[94]
Mean		86.6	6.9	13.6	17.7	106.7	57.7	
Std. dev.		0.8	0.7	2.3	0.6	0.8	0.7	
Rel. Std. Dev. (%)		0.9	9.8	17.2	3.4	0.7	1.2	

simulations. In a similar spirit as before, mean values are calculated here to provide benchmark values that can be compared to experimental values in order to reveal possible trends typical for calculated values obtained via computer simulations, and standard deviations should be considered as measures for the current reliability (not the precision) of these results in comparison to experimental results.

It is evident that the differences between individual simulation results are much larger than the differences between experimental measurements. The uncertainty of simulation results is clearly higher than that of experimental measurements (if the latter are performed correctly). It is also obvious that, while results of the early age of computer simulations (the late 1980s and early 1990s, say) must of course be considered with due caution, even more recent results do not automatically guarantee higher precision. In fact, many (on a more subtle level all) simulation results are in the end biased by experimental data, and coincidence of simulation results with available experimental data should not be interpreted to offer alternative or better results, but rather to be a testground for the reliability of simulation procedures. As such, this kind of coincidence may give some confidence in simulation results for cases where experimental data are not (or not yet) available.

Tables 6 and 7 list the elastic moduli  $E$ ,  $G$  and  $K$ , and the Poisson ratio  $\nu$ , calculated for dense isotropic polycrystalline quartz aggregates, such as very pure and dense sandstones and well crystallized quartzites, using the Voigt-Reuss-Hill average from the experimentally measured and simulated quartz monocrystal stiffness tensor components listed in Tables 4 and 5, respectively.

Comparing Tables 6 and 7 it is evident that experimental Young's moduli are in the range 94.5 - 96.4 GPa ( $95.6 \pm 0.6$  GPa), while Young's moduli obtained via computer simulations are typically smaller (with one exception) and exhibit a wider range of values ( $89.2 \pm 7.2$  GPa, range 84.3 - 100.0 GPa). Similar conclusions hold for the shear and bulk moduli: for  $G$  the experimental values are in the range 43.4 - 45.0 GPa ( $44.1 \pm 0.5$  GPa), for  $K$  in the range 36.5 - 40.7 GPa ( $38.4 \pm 1.1$  GPa), while the values published from computer simulations are for  $G$  in the range 38.7 - 45.1 GPa ( $40.3 \pm 3.0$  GPa) and for  $K$  in the range 30.7 - 42.6 GPa ( $38.3 \pm 4.9$  GPa). An early simulation result for  $K$ , not mentioned in this table, is 33.7 GPa [114], a value which lies very well within the range calculated here. The Poisson ratio calculated from experimentally measured elastic moduli is in the range 0.063 - 0.106 ( $0.084 \pm 0.011$ ), while that from computer simulations is in the range 0.041 - 0.132 ( $0.108 \pm 0.030$ ). Low-quartz densities resulting from simulations are in the range 2.48 - 2.76 g/cm<sup>3</sup> [114, 117, 119, 120], which is in satisfactory agreement with the commonly reported experimental value of 2.65 g/cm<sup>3</sup> at room temperature and can be considered as basic evidence for the success of the simulations.

The elastic constants of quartz undergo pronounced changes in the vicinity of the low-to-high-quartz transition at 573°C. The first comprehensive investigation of the temperature dependence of the elastic constants of quartz was performed by Perrier and de Mandrot [89], see also [1]. Since then, this temperature dependence has been investigated several times experimentally [75, 93, 122] and qualitatively confirmed via MD simulations [118].

Table 5. Independent components of the stiffness tensor [GPa] for low-quartz calculated via lattice dynamics (LD), molecular dynamics (MD) or density functional theory (DFT) for ambient pressure and temperatures at or around room temperature.

No.	Simulation method	$C_{11}$	$C_{12}$	$C_{13}$	$ C_{14} $	$C_{33}$	$C_{44}$	Reference
1	LD (empirical force field, rigid ion model)	191.9	113.0	140.4	0.0	198.4	42.0	[103]
2	LD (empirical force field, shell model)	94.7	18.3	19.6	14.5	116.0	50.0	[103]
3	MD (TTAM potential)	71.7	8.7	11.7	14.3	90.9	40.3	[116]
4	MD (ab initio, BKS potential)	90.5	8.1	15.2	17.6	107.0	50.2	[116]
5	MD (BKS potential)	86.4	-2.4	4.0	(-) 17.1	92.8	43.0	[117]
6	LD	90	6	14	18	100	45	[121]
7	DFT (ab initio, LDA with PWPP)	90	12	21	(-) 12	97	61	[119]
8	DFT (LDA with PAW)	87.2	15.4	17.8	16.2	108.6	54.8	[112]
9	DFT (KA pseudo-potential)	76.2	11.9	11.2	(-) 17.0	101.7	54.0	[120]
10	DFT (FHI pseudo-potential)	79.5	9.73	9.54	(-) 18.9	101.7	55.5	[120]
Mean	(without No. 1)	85.1	9.7	14.0	16.2	101.7	50.4	
Std. dev.	(without No. 1)	7.2	5.6	5.3	2.1	7.5	6.3	
Rel. std. dev. (%)	(without No. 1)	8.4	57.7	37.9	13.0	7.4	12.5	
Diff. to exp. data		-1.5	+2.8	+0.4	-1.5	-5.0	-7.3	
Rel. dev. from exper. data (%)	(without No. 1)	-1.7	+40.6	+2.9	-8.5	-4.7	-12.7	

Table 6. Elastic constants of isotropic polycrystalline low-quartz aggregates at and around room temperature, calculated from the experimentally measured stiffness tensor components in Table 4 (Voigt-Reuss-Hill averages).

No.	Type of constant (experimental method)	$E$ (GPa)	$G$ (GPa)	$K$ (GPa)	$\nu$ (1)	Based on reference
1	Isothermal (static)	94.54	43.56	38.10	0.086	[85]
2	Adiabatic (calculated from 1)	94.73	43.56	38.39	0.088	[1], based on [85]
3	Adiabatic isagric (resonant frequency)	95.51	44.49	37.44	0.074	[86, 87]
4	Adiabatic (resonant frequency)	95.60	45.01	36.49	0.063	[88]
5	Adiabatic (calculated from isothermal)	96.34	44.11	39.47	0.093	[1], based on [89]
6	n.a.	96.08	44.04	39.24	0.091	[90]
7	Adiabatic (ultrasonic wave velocities)	95.98	43.44	40.62	0.106	[91]
8	n.a.	95.66	44.44	37.75	0.077	[92]
9	Adiabatic (resonant frequency)	96.44	44.82	38.03	0.077	[93]
10	Adiabatic (Brillouin scattering)	95.33	43.99	38.26	0.084	[94]
Mean		95.6	44.1	38.4	0.084	
Std. dev.		0.6	0.5	1.1	0.011	
Rel. std. dev. (%)		0.6	1.1	2.9	13.1	

Table 7. Elastic constants of isotropic polycrystalline low-quartz aggregates at and around room temperature, calculated from the stiffness tensor components obtained from computer simulations listed in Table 5 (Voigt-Reuss-Hill averages).

No.	Simulation method	$E$ (GPa)	$G$ (GPa)	$K$ (GPa)	$\nu$ (1)	Based on reference
1	LD (empirical force field, rigid ion model)	100.8	36.3	151.3	0.389	[103]
2	LD (empirical force field, shell model)	96.5	41.9	46.5	0.154	[103]
3	MD (TTAM potential)	74.6	33.3	32.9	0.122	[116]
4	MD (ab initio, BKS potential)	93.4	42.0	40.3	0.113	[116]
5	MD (BKS potential)	84.3	40.5	30.7	0.041	[117]
6	LD	88.6	39.7	38.5	0.116	[121]
7	DFT (ab initio, LDA with PWPP)	100.0	45.1	42.6	0.109	[119]
8	DFT (LDA with PAW)	93.7	41.4	42.5	0.132	[112]
9	DFT (KA pseudo-potential)	85.1	38.7	35.6	0.100	[120]
10	DFT (FHI pseudo-potential)	86.7	40.1	34.8	0.083	[120]
Mean	(without No. 1)	89.2	40.3	38.3	0.108	
Std. dev.	(without No. 1)	7.2	3.0	4.9	0.030	
Rel. std. dev. (%)	(without No. 1)	8.1	7.4	12.8	27.8	
Diff. to exp. data		-6.4	-3.8	-0.1	+0.024	
Rel. dev. from exper. data (%)	(without No. 1)	-6.7	-8.6	-0.3	+28.6	

Table 8. Independent components of the stiffness tensor for high-quartz at 600°C (GPa); No. 1-3: experimental data, No. 4: computer simulation.

No.	Type of constant (method)	$C_{11}$	$C_{12}$	$C_{13}$	$C_{33}$	$C_{44}$	Reference
1	Adiabatic (resonant frequency)	118.4	19.0	32.0	107.0	35.8	[123, 124]
2	Adiabatic (resonant frequency)	112.5	12.5	26	103	37.5	[122]
3	Adiabatic (Brillouin scattering)	115	12	32.6	106.9	35.7	[75]
4	MD (BKS potential)	129	31	46	114	37.5	[118]
Mean	(without No. 4)	115.3	14.5	30.2	105.6	36.3	
Std. dev.	(without No. 4)	2.4	3.2	3.0	1.9	0.8	
Rel. std. dev. (%)	(without No. 4)	2.1	22.1	9.9	1.8	2.2	
Diff. to exp. data		+13.5	+16.5	+15.8	+8.4	+1.2	
Rel. dev. from exper. data (%)		+11.9	+113.8	+52.3	+8.0	+3.3	

Table 9. Elastic constants of isotropic polycrystalline high-quartz aggregates at 600°C, calculated from the stiffness tensor components obtained from published experimental data and computer simulation results listed in Table 8 (Voigt-Reuss-Hill averages).

No.	Type of constant (method)	$E$ (GPa)	$G$ (GPa)	$K$ (GPa)	$\nu$ (1)	Based on reference
1	Adiabatic (resonant frequency)	99.39	41.15	56.64	0.208	[123, 124]
2	Adiabatic (resonant frequency)	99.05	42.16	50.77	0.175	[122]
3	Adiabatic (Brillouin scattering)	98.71	41.20	54.51	0.198	[75]
4	MD (BKS potential)	102.4	40.9	68.7	0.251	[118]
Mean	(without No. 4)	99.1	41.5	54.0	0.194	
Std. dev.	(without No. 4)	0.3	0.5	2.4	0.014	
Rel. std. dev. (%)	(without No. 4)	0.3	1.2	4.4	7.2	
Diff. to exp. data		+ 3.3	- 0.6	+ 14.7	+ 0.057	
Rel. dev. from exper. data (%)		+ 3.3	- 1.4	+ 27.2	+ 29.4	

Table 8 lists published values for high-quartz at 600°C.

In contrast to the general conclusion for low-quartz, the available MD simulation results for high-quartz are higher than the published experimental data. The same is true for the elastic constants  $E$ ,  $K$  and  $\nu$  of isotropic polycrystalline high-quartz aggregates at this temperature (600°C), while the value of  $G$  obtained from the simulation is slightly below that calculated from published experimental data, see Table 9.

Figures 5 and 6 show the temperature dependence of the elastic moduli  $E$ ,  $G$  and  $K$ , and the Poisson ratio  $\nu$ , of quartz from 20 to 1050°C. The values have been calculated from stiffness tensor components measured via Brillouin scattering (Brillouin spectroscopy) [75]. It is evident that below 573°C the Young modulus and the bulk modulus exhibit a nonlinear decrease which parallels the decrease in density shown in Figure 7. At the transition temperature between low- and high-quartz (573°C) both  $E$  and  $K$  exhibit a sharp minimum, in contrast to the shear modulus  $G$ , which remains more or less unchanged throughout the whole temperature range. Although there has been some controversy about the nature of this phase transition for some time, it is now widely acknowledged, that it is a displacive phase transition (and not e.g. an order-disorder transition with

preexisting low-quartz domains in the high-temperature phase) and that it can be modeled within the framework of Landau theory as a first-order phase transition [21, 118]. Above the transition temperature of 573°C the Young modulus and the bulk modulus increase first very steeply, then (from 600°C upwards) smoothly. This increase of elastic moduli with increasing temperature is remarkable, because with increasing temperature the density remains almost unchanged at 2.53 g/cm<sup>3</sup>, see Figure 7. Due to the fact that the shear modulus remains constant, while the other two elastic moduli

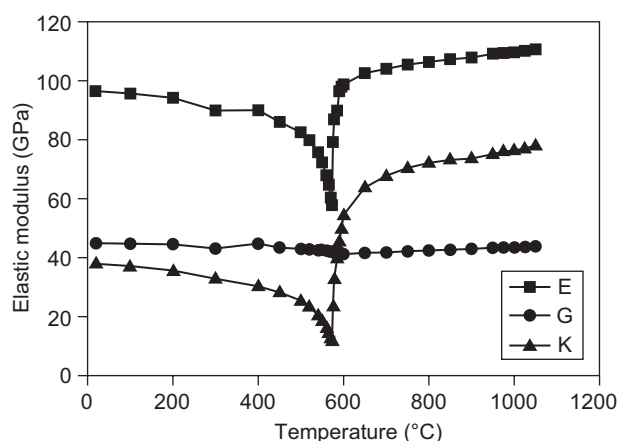


Figure 5. Temperature dependence of the elastic moduli  $E$ ,  $G$  and  $K$  of quartz, calculated from stiffness tensor components measured via Brillouin scattering [75].

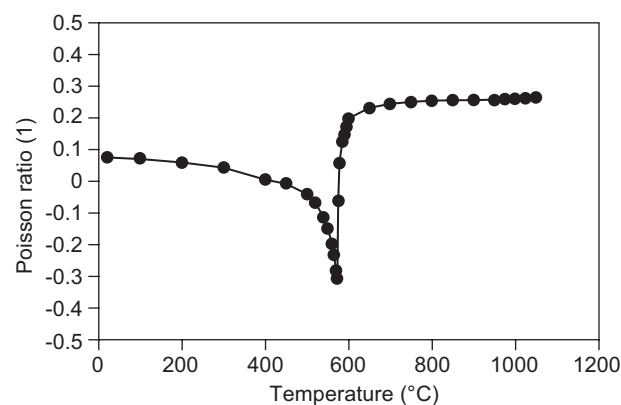


Figure 6. Temperature dependence of the Poisson ratio  $\nu$  of quartz, calculated from stiffness tensor components measured via Brillouin scattering [75].

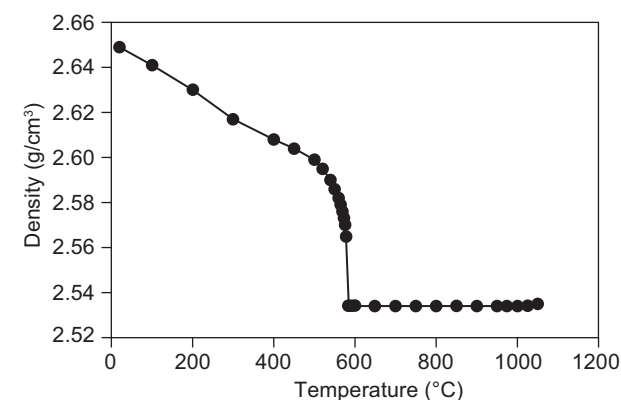


Figure 7. Temperature dependence of the density of quartz, based on the data in [75].

exhibit a sharp maximum, the Poisson ratio becomes negative in the temperature range 420 - 576.5°C. A similar temperature range of auxetic behavior of quartz (approx. 477 - 577°C) has also been reported elsewhere in the literature [93, 105, 110, 112]. In the temperature range from 650 to 1050°C the Poisson ratio and the shear modulus of high-quartz remain essentially constant ( $\nu$  increases from 0.232 to 0.264,  $G$  from 41.6 to 43.8 GPa), whereas the Young modulus and the bulk modulus increase considerably ( $E$  from 102.6 to 110.6 GPa,  $K$  from 63.8 to 78.0 GPa).

### Cristobalite

Similar to quartz, also cristobalite occurs in two modifications (low- and high-temperature subpolymorphs). The low-temperature modification is tetragonal (point group 422), and thus has 6 independent elastic constants (stiffness tensor components), while the high-temperature modification is cubic (point group  $4/m \bar{3} 2/m$ ) with only 3 independent elastic constants. In contrast to quartz, there seems to be only one experimental measurement available for the elastic constants of cristobalite, and this refers only to room temperature [63]. Therefore, results of computer simulations (MD and DFT-based) are very important in this case. Tables 10 and 11 list these results in comparison to the only published experimental data set for low-cristobalite at room temperature and for high-

cristobalite at high temperature, respectively.

Unfortunately, in the case of high-cristobalite the four data sets obtained by two teams of authors [110, 120] split up into two groups that are extremely different (apart from minor differences due to the potential chosen, which are negligible here), see Table 11. Thus, it must be surmised that one group is wrong. Similar conclusions hold for the elastic moduli elastic moduli  $E$ ,  $G$  and  $K$ , and the Poisson ratio  $\nu$ , see Tables 12 and 13. Of course, without further research a final decision cannot be made on this point. Nevertheless, the general modulus-versus-density correlation chart for silica phases given below (Figure 10) seems to suggest the conclusion that the simulation results reported by Kimizuka & Kaburaki [110] are more realistic. Moreover, also the earlier simulation result of 17.2 GPa for the bulk modulus obtained by Tsuneyuki et al. [114] is in reasonable agreement with the data set reported in [110] (but in serious disagreement with [120], see Table 13). Also the density calculated in [120] for high-cristobalite (1.97 g/cm<sup>3</sup>) is definitely too low, which is indicative of serious problems with these simulation results. On the other hand, low-cristobalite densities resulting from simulations are in the range 2.37 - 2.41 g/cm<sup>3</sup> [114, 117, 120] are slightly higher than the commonly reported experimental value of 2.32 g/cm<sup>3</sup> [125, 126].

It is evident that for low-cristobalite the Poisson ratio is negative at room temperature, i.e. isotropic poly-

Table 10. Independent components of the stiffness tensor (GPa) for low-cristobalite measured experimentally and calculated via molecular dynamics (MD) or density functional theory (DFT) for ambient pressure at or around room temperature.

No.	Method	$C_{11}$	$C_{12}$	$C_{13}$	$C_{33}$	$C_{44}$	$C_{66}$	Reference
1	Brillouin scattering	59.4	3.8	-4.4	42.4	67.2	25.7	[63]
2	MD (BKS potential)	55.7	4.2	10.5	33.2	70.7	30.6	[117]
3	MD (TTAM potential)	48.1	5.6	-4.2	35.3	57.8	19.8	[109-111]
4	MD (BKS potential)	64.5	6.5	-0.7	37.9	69.5	27.6	[109-111]
5	DFT (LDA with PAW)	54.6	5.2	-7.4	36.4	68.6	25.0	[111, 112]
6	DFT (KA pseudo-potential)	49.3	5.3	-11.4	44.8	74.2	26.9	[120]
Mean	(without No. 1)	54.4	5.4	-2.6	37.5	68.2	26.0	
Std. dev.	(without No. 1)	5.8	0.7	7.5	3.9	5.5	3.6	
Rel. std. dev. (%)	(without No. 1)	10.7	13.0	288.5	10.4	8.1	13.8	
Diff. to exp. data		-5.0	+1.6	(+) 1.8	-4.9	+1.0	+0.3	
Rel. dev. from exper. data (%)		-8.4	+42.1	(+) 40.9	-11.6	+1.5	+1.2	

Table 11. Independent components of the stiffness tensor [GPa] for high-cristobalite calculated via molecular dynamics (MD) or density functional theory (DFT) for ambient pressure.

No.	Method	$C_{11}$	$C_{12}$	$C_{44}$	Reference
1	MD (TTAM potential, 1527°C)	42.0	5.8	40.8	[110]
2	MD (BKS potential, 1527°C)	49.6	5.7	49.7	[110]
3	DFT (KA pseudo-potential)	194.0	135.0	82.67	[120]
4	DFT (FHI pseudo-potential)	196.1	134.2	85.40	[120]
Mean	(without No. 3 and 4)	45.8	5.8	45.3	
Std. dev.	(without No. 3 and 4)	5.4	0.1	6.3	
Rel. std. dev. (%)	(without No. 3 and 4)	11.7	1.2	13.9	

crystalline aggregates of low-cristobalite, e.g. fired silica refractory bricks without residual quartz and with a negligible tridymite content, should exhibit auxetic behavior. Auxetic behavior has been confirmed also by theoretical (analytical) model calculations [127] and different mechanisms have been devised to account for this behavior [128]. For high-cristobalite the situation is not so clear, see Table 13. Figures 8 and 9 show the temperature dependence of the elastic moduli  $E$ ,  $G$  and

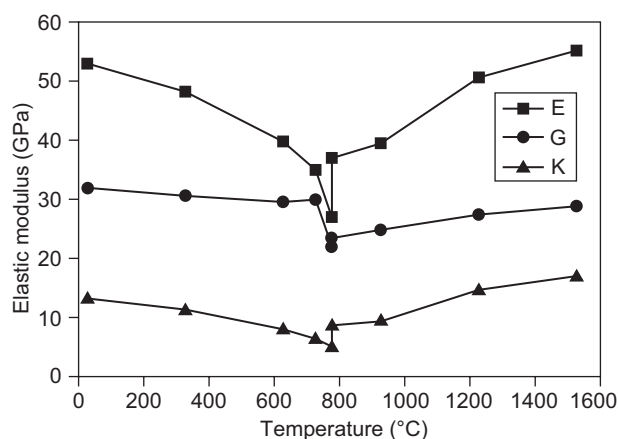


Figure 8. Temperature dependence of the elastic moduli  $E$ ,  $G$  and  $K$  of cristobalite, according to the MD simulations of Kimizuka and coworkers [109, 110].

$K$ , and the Poisson ratio  $\nu$ , respectively, according to the MD simulations of Kimizuka and coworkers [109, 110]. According to these results, the Poisson ratio remains negative in the whole range of temperatures from room temperature up to more than 1500°C, i.e. low- and high-cristobalite are both auxetic. However, it is evident that the transition temperature between low- and high-cristobalite predicted by this MD simulation (777°C) is much higher than the experimental values commonly reported, which are usually somewhere in the range

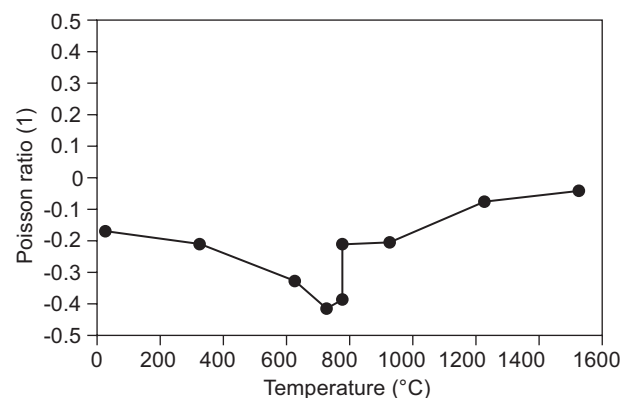


Figure 9. Temperature dependence of the Poisson ratio  $\nu$  of cristobalite, according to the MD simulations of Kimizuka and coworkers [109, 110].

Table 12. Elastic constants of isotropic polycrystalline low-cristobalite aggregates at or around room temperature, calculated from the stiffness tensor components obtained from published experimental data and computer simulation results listed in Table 10 (Voigt-Reuss-Hill averages).

No.	Method	$E$ (GPa)	$G$ (GPa)	$K$ (GPa)	$\nu$ (1)	Based on reference
1	Brillouin scattering	65.2	39.1	16.4	-0.164	[63]
2	MD (BKS potential)	68.14	35.60	21.32	-0.037	[117]
3	MD (TTAM potential)	53.85	32.14	13.62	-0.161	[109-111]
4	MD (BKS potential)	69.64	39.49	18.83	-0.117	[109-111]
5	DFT (LDA with PAW)	58.52	38.02	13.39	-0.229	[111, 112]
6	DFT (KA pseudo-potential)	56.34	40.40	11.77	-0.300	[120]
Mean	(without No. 1)	61.3	37.1	15.8	-0.169	
Std. dev.	(without No. 1)	6.4	3.0	3.7	0.091	
Rel. std. dev. (%)	(without No. 1)	10.4	8.0	23.1	53.8	
Diff. to exp. data		-3.9	-2	-0.6	(-) 0.005	
Rel. dev. from exper. data (%)		-6.0	-5.1	-3.7	(-) 3.0	

Table 13. Elastic constants of isotropic polycrystalline high-cristobalite aggregates, calculated from the stiffness tensor components obtained from published computer simulation results listed in Table 11 (Voigt-Reuss-Hill averages).

No.	Method	$E$ (GPa)	$G$ (GPa)	$K$ (GPa)	$\nu$ (1)	Based on reference
1	MD (TTAM potential, 1527°C)	56.94	29.44	17.89	-0.032	[110]
2	MD (BKS potential, 1527°C)	67.59	35.80	20.33	-0.055	[110]
3	DFT (KA pseudo-potential)	146.64	54.72	154.67	0.341	[120]
4	DFT (FHI pseudo-potential)	151.80	56.87	154.83	0.336	[120]
Mean	(without No. 3 and 4)	62.3	32.6	19.1	-0.044	
Std. dev.	(without No. 3 and 4)	7.5	4.5	1.7	0.016	
Rel. std. dev. (%)	(without No. 3 and 4)	12.1	13.8	9.0	37.4	

200 - 280°C [9]. Although similar tendencies are sometimes reported for pair potentials [129], such a large discrepancy might indicate a more principal problem with these MD simulation results. Nevertheless, these results indicate that the elastic moduli decrease with increasing temperature until the transition temperature and then they exhibit a steep increase followed by a smooth increase up to the highest temperatures studied. Immediately below and above the transition temperature they attain approximately the same level. In particular, the Young modulus exhibits a temperature dependence which is qualitatively similar to quartz (except for the absolute values, which are clearly lower, and the position of the transition temperature, which is wrong due to a computational artefact). In contrast to quartz, in the case of cristobalite also the shear modulus shows a sharp discontinuity at the transition temperature. For all elastic constants of cristobalite the decrease is relatively smooth when the transition temperature is approached from below and extremely steep (steeper than for quartz) when it is approached from above. A specific point that is not visible from these MD simulation data, is the large hysteresis of the cristobalite transformation, which can be up to  $\pm 30^\circ\text{C}$  about the equilibrium temperature between heating and cooling [128] and is a consequence of the fact that this transition is kinetically controlled and relatively sluggish, see also [117].

#### Stishovite and other silica polymorphs

The enormous interest in the elastic properties of quartz during the 20<sup>th</sup> century was triggered by the utmost importance of quartz single crystals for piezoelectric applications, while the elastic properties of cristobalite become a focus of research towards the end of the 20<sup>th</sup> century after the discovery of isotropic auxetic materials and the finding that cristobalite is one of the few materials, whose isotropic polycrystalline aggregates could be auxetic even when dense, i.e. without the

necessity of a pore space with a specific microstructure (as in the case of most auxetic polymers). For more than two decades now, computer simulations are used to provide information confirming or complimentary to experimental measurements.

Although the temperature dependence of the elastic constants has become an issue in the second half of the 20<sup>th</sup> century especially in the geological and geophysical community, because the transition from low- to high-quartz is of general interest there, experimental data for the temperature dependence of the elastic constants (single crystal stiffness tensor components) for cristobalite are missing so far, so that e.g. for high-cristobalite only simulation results are available.

Compared to quartz and cristobalite, the situation for other silica polymorphs is much worse. However, for stishovite monocrystals (tetragonal, point group 4/mmm, space group  $P4_2/mnm$ ), the highest-density silica polymorph (density 4.28 - 4.35 g/cm<sup>3</sup>) [10, 130], experimentally measured data are available for the stiffness tensor components, at least at room temperature [131]. Table 14 lists these data in comparison with more recent simulation results [117, 120].

It is evident that the early MD simulation results [117] are relatively far off the experimental values, while the newer DFT results [119, 120] are in excellent agreement, indicating that the pseudopotentials chosen are very realistic in this case. Therefore, we would recommend the (average of the) data sets 1, 3, 4 and 5 as current “state-of-the-art“ mean values. The same holds true for the elastic moduli  $E$ ,  $G$  and  $K$ , and the Poisson ratio  $\nu$ , listed in Table 15. Early experimental and simulation results for  $K$ , not mentioned in this table, are 335 GPa [132] and 311 GPa [114], respectively, which is in reasonable agreement with the values calculated here. Stishovite densities resulting from simulations are in the range 3.98 - 4.31 g/cm<sup>3</sup> [114, 117, 119], which is close to the experimental values commonly reported, viz. 4.28 - 4.35 g/cm<sup>3</sup> [10, 130].

In contrast to stishovite, the elastic moduli of coesite are not very well known. However, the bulk modulus

Table 14. Independent components of the stiffness tensor (GPa) for stishovite measured experimentally and calculated via molecular dynamics (MD) or density functional theory (DFT) for ambient pressure at or around room temperature.

No.	Method	$C_{11}$	$C_{12}$	$C_{13}$	$C_{33}$	$C_{44}$	$C_{66}$	Reference
1	Adiabatic (resonant frequency)	453	211	203	776	252	302	[131]
2	MD (BKS potential)	703	314	281	1072	287	260	[117]
3	DFT (ab initio, LDA with PWPP)	480	245	220	735	260	340	[119]
4	DFT (KA pseudo-potential)	447.7	211.0	203.0	776.0	252.0	302.0	[120]
5	DFT (FHI pseudo-potential)	448.8	211.1	191.0	752.0	256.5	323.0	[120]
Mean	(without 1 and 2)	458.8	222.4	204.7	754.3	256.2	321.7	
Std. dev.	(without 1 and 2)	18.3	19.6	14.6	20.6	4.0	19.0	
Rel. std. dev. (%)	(without 1 and 2)	4.0	8.8	7.1	2.7	1.6	5.9	
Diff. to exp. data		+ 5.8	+ 11.4	+ 1.7	- 21.7	+ 4.2	+ 19.7	
Rel. dev. from exper. data (%)		+ 1.3	+ 5.4	+ 0.8	- 2.8	+ 1.7	+ 6.5	

Table 15. Elastic constants of isotropic polycrystalline stishovite aggregates, calculated from the stiffness tensor components obtained from published computer simulation results listed in Table 14 (Voigt-Reuss-Hill averages).

No.	Method	$E$ (GPa)	$G$ (GPa)	$K$ (GPa)	$\nu$ (1)	Based on reference
1	Adiabatic (resonant frequency)	536.2	220.3	316.1	0.217	[131]
2	MD (BKS potential)	675.2	268.5	463.8	0.257	[117]
3	DFT (ab initio, LDA with PWPP)	550.8	224.6	336.1	0.227	[119]
4	DFT (KA pseudo-potential)	533.2	219.0	314.7	0.218	[120]
5	DFT (FHI pseudo-potential)	540.0	224.0	308.7	0.208	[120]
Mean	(without 1 and 2)	541.3	222.5	319.8	0.218	
Std. dev.	(without 1 and 2)	8.9	3.1	14.4	0.010	
Rel. std. dev. (%)	(without 1 and 2)	1.6	1.4	4.5	4.4	
Diff. to exp. data		+ 5.1	+ 2.2	+ 3.7	+ 0.001	
Rel. dev. from exper. data (%)		+ 1.0	+ 1.0	+ 1.2	+ 0.3	

of coesite is reported to be 96.3 GPa (experimental value) or 108 GPa (simulation result) [114], while densities obtained from simulation results (2.72 g/cm<sup>3</sup>) are considerably smaller than commonly reported experimental density values (2.92 - 3.0 g/cm<sup>3</sup>).

General trends and recommended values for the elastic constants of dense isotropic polycrystalline aggregates of crystalline silica polymorphs and of silica glass

Figure 10 shows in graphical form the dependence of the elastic moduli  $E$ ,  $G$  and  $K$  on the density of silica phases. It is evident that there is a clear correlation between elastic moduli and density, which can be expected on physical grounds and may be used for rough estimates or interpolation purposes. For obvious reasons no such correlation chart is available for the Poisson ratio. However, for the elastic moduli  $E$ ,  $G$  and  $K$  this chart provides

reasonable guidelines for estimating elastic moduli of silica phases for which neither experimental nor simulation results are available, e.g. tridymite. Based on this correlation and the corresponding fit curves, the elastic moduli  $E$ ,  $G$  and  $K$  of low-tridymite (density 2.26 g/cm<sup>3</sup>) can be estimated to be 58.1, 28.8 and 20.2 GPa, respectively, while the corresponding moduli of high-tridymite (density 2.22 g/cm<sup>3</sup>) can be estimated to be 52.8, 26.7 and 17.0 GPa, respectively. Based on these values the Poisson ratio expected are in the range from + 0.009 to + 0.021 for low-tridymite and in the range from - 0.011 to - 0.018 for high-tridymite. Of course, this is not a proof that high-tridymite is auxetic (although it is a possible candidate for such behavior), but what can be said is that the Poisson ratio of tridymite is probably very close to zero.

Based on the data collected and compared in this paper, we recommend the elastic constant values listed in Table 16, including estimates for tridymite based on the before mentioned modulus-density correlation. In order to obtain internally consistent data sets, the values

Table 16. Recommended values for the elastic constants of dense isotropic polycrystalline aggregates of crystalline silica polymorphs (and silica glass), calculated from the mean values for the tensile and shear moduli listed in the tables above (for tridymite interpolated from the modulus-density correlation chart).

Silica phase	Method	Density (g/cm <sup>3</sup> )	$E$ (GPa)	$G$ (GPa)	$K$ (GPa)	$\nu$ (1)
Glass	Experiment	2.20	72.2	30.9	36.3	0.168
Low-quartz	Experiment	2.65	95.6	44.1	38.3	0.084
	Simulation		89.2	40.3	37.8	0.107
High-quartz	Experiment	2.53	99.1	41.5	54.0	0.194
	Simulation		102.4	40.9	68.8	0.252
Low-cristobalite	Experiment	2.32	65.2	39.1	16.3	- 0.166
	Simulation		61.3	37.1	15.2	- 0.174
High-cristobalite	Experiment	2.20	-	-	-	-
	Simulation		62.3	32.6	19.1	- 0.044
Low- tridymite	Estimate	2.26	58.1*	28.8*	19.7*	0.009*
High-tridymite	Estimate	2.22	52.8*	26.7*	17.2*	- 0.011*
Coesite	Experiment	≈ 3.0	-	-	96.3	-
	Simulation		-	-	108	-
Stishovite	Experiment	≈ 4.3	536.2	220.3	315.8	0.217
	Simulation		541.3	222.5	318.0	0.216

in this table have been calculated from the mean values for the tensile and shear moduli listed in the tables above (and for tridymite interpolated from Figure 10). Note that the average values of  $K$  and  $\nu$  listed in the tables before (and for tridymite interpolated from Figure 10) have been obtained by averaging independent results of different authors and therefore need not be exactly consistent with the  $K$  and  $\nu$  values calculated from the average values of  $E$  and  $G$ . Additionally, the data have been supplemented by two values (experimental and simulated) for the bulk modulus of coesite [114]. Data originating from computer simulations are listed for comparison and because they are in some cases the only available ones, but it is clear that experimental data should be preferred wherever available.

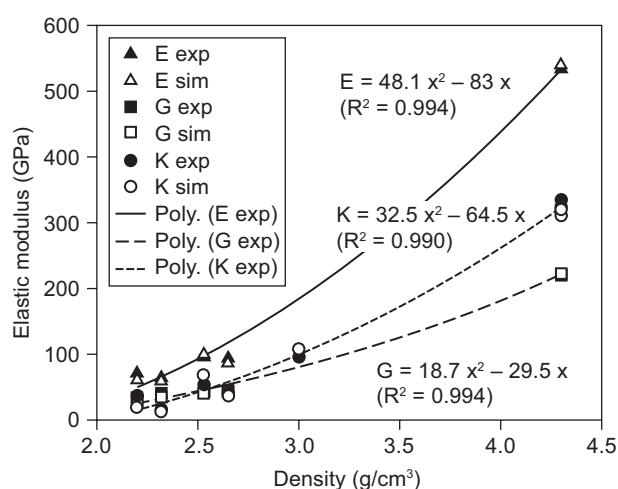


Figure 10. Dependence of the elastic moduli  $E$ ,  $G$  and  $K$  on the density of silica phases; data columns from left to right: silica glass and high-cristobalite (density  $2.20 \text{ g/cm}^3$ ), low-cristobalite (density  $2.32 \text{ g/cm}^3$ ), high-quartz (density  $2.53 \text{ g/cm}^3$ ), low-quartz (density  $2.65 \text{ g/cm}^3$ ), coesite (density  $\approx 3.0 \text{ g/cm}^3$ ) and stishovite (density  $\approx 4.3 \text{ g/cm}^3$ ) [114, 132]; experimental data fitted by second-order fit curves ( $x$  = density, correlation coefficient  $> 0.99$ ).

## CONCLUSIONS

The elastic properties of silica phases have been reviewed. Available monocrystal data for crystalline  $\text{SiO}_2$  polymorphs (low-quartz, high-quartz, low-cristobalite, high-cristobalite, stishovite) have been collected from the literature, and effective elastic constants (Young's moduli, shear moduli, bulk moduli and Poisson ratios) have been calculated from these using Voigt-Reuss-Hill averaging. Both experimental data and simulation results have been taken into account. Based on the data collected in this paper, a table of room temperature elastic constants for crystalline silica polymorphs and silica glass has been given that lists the values that can be recommended as the current "state-of-the-art" values. All data are consistent with the well-known

auxetic behavior of cristobalite at room temperature. Moreover, high-temperature simulation data published for cristobalite seem to confirm the auxetic behavior of cristobalite for all temperatures from room temperature up to more than  $1500^\circ\text{C}$ . The calculations of this paper show that also quartz can be auxetic, but only in a very limited temperature range around the low-to-high-quartz transition temperature ( $420 - 577^\circ\text{C}$ ). Except for silica glass and quartz, however, high-temperature experimental data are virtually non-existent so far, and especially the behavior of elastic constants in the vicinity of phase transitions is largely unknown and cannot be reliably simulated. Even worse is the situation for tridymite, for which even reliable room temperature data are lacking. Therefore, experimental measurements of elastic properties of tridymite and cristobalite, including high-temperature measurements, must still be considered an urgent desideratum of current research.

## Acknowledgements

This work was part of the project "Porous ceramics with tailored elasticity and thermal conductivity" (GAČR project No. P108/12/1170), supported by the Czech Science Foundation (Grantová agentura České republiky).

## REFERENCES

1. Cady W.G.: *Piezoelectricity*, p. 1-159. McGraw-Hill, New York 1946.
2. Petzold A.: *Physikalische Chemie der Silicate und nicht-oxidischen Siliciumverbindungen* (Physical Chemistry of Silicates and Nonoxide Silicon Compounds, in German), p. 91-99. Deutscher Verlag für Grundstoffindustrie, Leipzig 1991.
3. Salmang H., Scholze H.: *Keramik – Volume I* (6<sup>th</sup> edition), p. 36-41, 117-122, 186-195. Springer-Verlag, Berlin 1982.
4. Sosman R.B.: *Trans. Br. Ceram. Soc.* 54, 655 (1955).
5. Sosman R.B.: *The Phases of Silica*. Rutgers University Press, New Brunswick 1965.
6. Brückner R.: *J. Non-Cryst. Solids* 5, 123 (1970).
7. Fanderlík I.: *Silica Glass and its Applications* (= Glass Science and Technology Vol. 11), p. 21-38, 206-216. Elsevier, Amsterdam 1991.
8. Deer W.A., Howie R.A., Zussman J.: *An Introduction to the Rock-Forming Minerals*, p. 340-355. Longman, London 1966.
9. Greenwood N.N., Earnshaw A.: *Chemie prvků – Volume I*, p. 415-419. Informatorium, Prague 1993.
10. Klein C., Hurlbut C.S.: *Manual of Mineralogy* (20<sup>th</sup> edition), p. 437-444. John Wiley & Sons, New York 1985.
11. Bárta R.: *Chemie a technologie cementu* (Chemistry and Technology of Cements, in Czech), p. 80-81, 946. Nakladatelství československé akademie věd, Prague 1961.
12. Flörke O.W., Müller-Vonmoos M.: *Z.Kristallogr.* 133, 193 (1971).
13. Kihara K.: *Z.Kristallogr.* 148, 237 (1978).

14. Hill V.B., Roy R.: *Trans. Br. Ceram. Soc.* 57, 596 (1958).
15. Rockett T.J., Foster W.R.: *Am. Mineral.* 52, 1233 (1967).
16. Eitel W.: *Bull. Am. Ceram. Soc.* 36, 142 (1957).
17. Flörke O.W.: *Naturwiss.* 43, 419 (1956).
18. Flörke O.W.: *Fortschr. Min.* 44, 181 (1967).
19. Holmquist S.B.: *Am. Mineral.* 53, 501 (1968).
20. Carpenter M.A., Wennemer M.: *Am. Mineral.* 70, 517 (1985).
21. Heimann R.B.: *Classic and Advanced Ceramics*, p. 71-81, 507-520. Wiley-VCH, Weinheim 2010.
22. Flörke O.W.: *Fortschr. Min.* 32, 33 (1953).
23. Holmquist S.B.: *J. Am. Ceram. Soc.* 44, 82 (1961).
24. Wollast A.F.: *Sci. Ceram.* 3, 29 (1967).
25. Petzold A.: *Anorganisch-nichtmetallische Werkstoffe – Charakteristik, Eigenschaften, Anwendungsverhalten* (Inorganic-Nonmetallic Materials – Characteristics, Properties, Performance, in German), p. 53, 161-164. Deutscher Verlag für Grundstoffindustrie, Leipzig 1981.
26. Schulle W.: *Feuerfeste Werkstoffe* (Refractory Materials, in German), p. 168-184. Deutscher Verlag für Grundstoffindustrie, Leipzig 1990.
27. Staroň J., Tomšů F.: *Žiaruvzdorné materiály – výroba, vlastnosti a použitie* (Refractory Materials – Production, Properties and Application, in Slovakian), p. 104-122. Slovomag / Slovenské magnezitové závody / Keramika, Lubeník / Jelšava / Košice 2000.
28. Chvátal M.: *Úvod do systematické mineralogie* (Introduction to Systematic Mineralogy, in Czech), p. 39-41. Silikátový svaz, Prague 2005.
29. Rösler H.J.: *Lehrbuch der Mineralogie* (Textbook of Mineralogy, in German), 3<sup>rd</sup> edition, p. 437-453. Deutscher Verlag für Grundstoffindustrie, Leipzig 1984.
30. Coes L.: *Science* 118, 131 (1953).
31. Stishov S.M., Popova S.V.: *Geokhimiya* 10, 837 (1961).
32. Keat P.P.: *Science* 129, 328 (1954).
33. Weiss A., Weiss A.: *Naturwiss.* 41, 12 (1954).
34. Belonoshko A.B., Dubrovinsky L.S., Dubrovinsky N.A.: *Am. Mineral.* 81, 785 (1996).
35. Carpenter M.A., Hemley R.J., Mao H.K.: *J. Geophys. Res.* 105, 10807 (2000).
36. Flörke O.W., Jones J.B., Schminke H.U.: *Z. Kristallogr.* 143, 156 (1976).
37. Buerger M.J.: *Crystallographic aspects of phase transformations*, in Smoluchowski R., Mayer J.E., Weyl W.A. (eds.): *Phase Transformations in Solids*. John Wiley & Sons, New York 1951.
38. Heuer A.H.: *J. Am. Ceram. Soc.* 58, 529 (1975).
39. Fenner C.N.: *Am. J. Sci.* 36, 331 (1913).
40. Mitra S.: *Trans. Br. Ceram. Soc.* 76, 74 (1977).
41. Baumgart W. in: *Process Mineralogy of Ceramic Materials*, p. 82-84, Eds. Baumgart W., Dunham A.C., Amstutz G.C., Ferdinand Enke, Stuttgart 1984.
42. DeKeyser W.L., Cyprès R.: *Ber. Dtsch. Keram. Ges.* 38, 303 (1961).
43. Madden G.J., van Vlack L.H.: *J. Am. Ceram. Soc.* 50, 414 (1967).
44. Schulle W.: *Silikattechn.* 22, 312 (1972).
45. Elstner I., Leistner H. in: *Keramik – Volume 2* (6<sup>th</sup> edition), p. 116-165, Eds. Salmang H., Scholze H., Springer, Berlin 1982.
46. Flörke O.W.: *Ber. Dtsch. Keram. Ges.* 34, 343 (1957).
47. Leadbetter A.J., Wright A.F., Smith T.W.: *Phil. Mag.* 33, 105 (1976).
48. Wright A.F.: *Am. Ceram. Soc. Bull.* 56, 718 (1977).
49. Blažek A.: *Termická analýza* (Thermal Analysis, in Czech), p. 194-195. SNTL, Prague 1974.
50. Arnold H.: *Z. Kristallogr.* 121, 145 (1965).
51. Gibbs R.E.: *Proc. Roy. Soc. A* 113, 351 (1927).
52. Flörke O.W.: *Ber. Dtsch. Keram. Ges.* 32, 369 (1955).
53. Heimann R.B.: *Miner. Sci. Eng.* 9, 57 (1977).
54. Dove M.T., Keen D.A., Hannon A.C., Swainson I.P.: *Phys. Chem. Miner.* 24, 311 (1997).
55. Dove M.T., Trachenko K.O., Tucker M.G., Keen D.A. in: *Transformation Processes in Minerals* (Reviews in Mineralogy & Geochemistry – Volume 39), p. 1-33, Eds. Redfern S. A. T., Carpenter M. A., Mineralogical Society of America, Washington 2000.
56. Kitchin S.J., Kohn S.C., Dupree R., Henderson C.M., Kihara K.: *Am. Mineral.* 81, 550 (1996).
57. Konnerth J.H., Appelman D.E.: *Acta Crystallogr. B* 34, 391 (1978).
58. Dollase W.A.: *Acta Crystallogr.* 23, 617 (1967).
59. Nukui A., Nakazawa H., Akao M.: *Amer. Mineral.* 63, 1252 (1978).
60. Mackenzie J.D.: *J. Am. Ceram. Soc.* 43, 615 (1960).
61. Scherer G., Vergano P.J., Uhlmann D.R.: *Phys. Chem. Glasses* 11, 53 (1970).
62. Pabst W., Gregorová E.: *Ceram.-Silik.* 47, 1 (2003).
63. Yeganeh-Haeri A., Weidner D.J., Parise J.B.: *Science* 257, 650 (1992).
64. Pabst W., Gregorová E., Tichá G., Týnová E.: *Ceram.-Silik.* 48, 41 (2004).
65. Pabst W., Gregorová E. in: *Ceramics and Composites: New Research*, p.31-100, Ed. Caruta, B. M., Nova Science Publishers, New York 2006.
66. Voigt W.: *Ann. Phys.* 38, 573 (1889).
67. Reuss A.: *Z. Angew. Math. Mech.* 9, 49 (1929).
68. Hill R.: *Proc. Roy. Soc. Lond. A* 65, 349 (1952).
69. Green D.J.: *An Introduction to the Mechanical Properties of Ceramics*, p. 78-98. Cambridge University Press, Cambridge 1998.
70. Pabst W.: *Ceram.-Silik.* 49, 254 (2005).
71. Pabst W., Gregorová E. in: *New Developments in Materials Science Research*, p.77-137, Ed. Caruta B. M., Nova Science Publishers, New York 2007.
72. Callen H.B.: *Thermodynamics*, p. 56, 234, 344. John Wiley & Sons, New York 1960.
73. Meyer K.: *Physikalisch-chemische Kristallographie* (2<sup>nd</sup> edition), p. 52-56. Deutscher Verlag für Grundstoffindustrie, Leipzig 1977.
74. Polian A., Vo-Thang D., Richet P.: *Europhys. Lett.* 57, 375 (2002).
75. Lakshtanov D.L., Sinogeikin S.V., Bass J.D.: *Phys. Chem. Minerals* 34, 11 (2007).
76. Volf M.B.: *Technical Approach to Glass* (= Glass Science and Technology Vol. 10), p. 19-37. Elsevier, Amsterdam 1990.
77. Dietzel A.: *Kolloid-Z.* 100, 368 (1942).
78. Gillod J.: *Verres Réfract.* 26, 33 (1948).
79. Spinner S.: *J. Am. Ceram. Soc.* 39, 113 (1956).
80. Spinner S.: *J. Am. Ceram. Soc.* 45, 394 (1962).
81. Menčík J.: *Strength and Fracture of Glass and Ceramics* (= Glass Science and Technology Vol. 12), p. 17-20. Elsevier, Amsterdam 1992.
82. Schill F.: *Chlazení skla* (Cooling of Glass, in Czech), p. 141-143. Informatorium, Prague 1993.

83. Frazer D.B.: J. Appl. Phys. 39, 5868 (1968).
84. Forte S., Vianello M.: J. Elasticity 43, 81 (1996).
85. Voigt W.: *Lehrbuch der Kristallphysik* (2<sup>nd</sup> edition), p. 752-753. Teubner, Leipzig 1928.
86. Atanasoff J.V., Hart P.J.: Phys. Rev. 59, 85 (1941).
87. Lawson A.W.: Phys. Rev. 59, 838 (1941).
88. Mason W.P.: Bell Systems Technical Journal 22, 178 (1943).
89. Perrier A., de Mandrot R.: Mém. Soc. Vaud. Sci. Nat. 1, 333 (1922).
90. Nye J. F.: *Physical Properties of Crystals*, p. 131-149. Clarendon Press, Oxford 1985.
91. McSkimin H.J., Andreatch P., Thurston R.N.: J. Appl. Phys. 36, 1624 (1965).
92. Haussühl S.: *Kristallphysik*, p. 419. Physik-Verlag, Weinheim 1983.
93. Ohno I.: J. Phys. Earth 43, 157 (1995).
94. Grimsditch M., Polian A., Brazhkin V., Balitskii D.: J. Appl. Phys. 83, 3018 (1998).
95. Giebe E., Scheibe A.: Ann. Phys. 9, 93 (1931).
96. Khol F.: Z. Phys. 108, 225 (1938).
97. Sosman R.B.: *The Properties of Silica* (856 pp.). Chemical Catalog Company, New York 1927.
98. Joffé A.F.: *The Physics of Crystals* (198 pp.). McGraw-Hill, New York 1928.
99. Parrinello M., Rahman A.: Phys. Rev. Lett. 45, 1196 (1980).
100. Parrinello M., Rahman A.: J. Chem. Phys. 76, 2662 (1982).
101. Hohenberg P., Kohn W.: Phys. Rev. B 136, 864 (1964).
102. Kohn W., Sham L.J.: Phys. Rev. A 140, 1133 (1965).
103. Jackson R.A., Catlow C.R.A.: Mol. Simul. 1, 207 (1988).
104. Smirnov M.B., Mirgorodsky A.P.: Phys. Rev. Lett. 78, 2413 (1997).
105. Zubov V.G., Firsova M.M.: Sov. Phys. Crystallogr. 7, 374 (1962).
106. Alderson A., Evans K.E.: Phys. Rev. Lett. 89, 225503 (2002).
107. Keskar N.R., Chelikowsky J.R.: Nature 358, 222 (1992).
108. Keskar N.R., Chelikowsky J.R.: Phys. Rev. B 48, 16227 (1993).
109. Kimizuka H., Kaburaki H., Kogure Y.: Phys. Rev. Lett. 84, 5548 (2000).
110. Kimizuka H., Kaburaki H.: Phys. Stat. Sol. B 242, 607 (2005).
111. Kimizuka H., Ogata S., Shibutani Y.: Mater. Trans. 46, 1161 (2005).
112. Kimizuka H., Ogata S., Shibutani Y.: Phys. Stat. Sol. B 244, 900 (2007).
113. Maddox J.: Nature 335, 201 (1988).
114. Tsuneyuki S., Tsukada M., Aoki H., Matsui Y.: Phys. Rev. Lett. 61, 869 (1988).
115. della Valle R.G., Andersen H.C.: J. Chem. Phys. 94, 5056 (1991).
116. van Beest B.W.H., Kramer G.J., van Santen R.A.: Phys. Rev. Lett. 64, 1955 (1990).
117. Tse J.S., Klug D.D.: J. Chem. Phys. 95, 9176 (1991).
118. Müser M.H., Binder K.: Phys. Chem. Miner. 28, 746 (2001).
119. Holm B., Ahuja R.: J. Chem. Phys. 111, 2071 (1999).
120. Sevik C., Bulutay C.: J. Mater. Sci. 42, 6555 (2007).
121. Purton J., Jones R., Catlow C.R.A., Leslie M.: Phys. Chem. Miner. 19, 392 (1993).
122. Carpenter M.A., Salje E.K.H., Graeme-Barber A., Wrucki B., Dove M.T., Knight K.S.: Am. Mineral. 83, 2 (1998).
123. Atanasoff J.V., Kammer E.W.: Phys. Rev. 59, 97 (1941).
124. Kammer E.W., Atanasoff J.V.: Phys. Rev. 62, 395 (1942).
125. Peacor D.R.: Z. Kristallogr. 138, 274 (1973).
126. Dollase W.A.: Z. Kristallogr. 138, 274 (1965).
127. Guo C.Y., Wheeler L.: J. Mech. Phys. Solids 54, 690 (2006).
128. Alderson A., Evans K.E.: J. Phys. Condens. Matter 21, 025401 (2009).
129. Bourova E., Parker S. C., Richet P.: Phys. Rev. B 62, 12052 (2000).
130. Tsuchida Y., Yagi T.: Nature 340, 217 (1989).
131. Weidner D.J., Bass J.D., Ringwood A.E., Sinclair W.: J. Geophys. Res. 87, 4740 (1982).
132. Levien L., Prewitt C.T.: Am. Mineral. 66, 324 (1981).